

2012

# Study of nanoparticle binding in a microfluidic platform

Antony Thomas  
*Lehigh University*

Follow this and additional works at: <http://preserve.lehigh.edu/etd>

---

## Recommended Citation

Thomas, Antony, "Study of nanoparticle binding in a microfluidic platform" (2012). *Theses and Dissertations*. Paper 1044.

This Thesis is brought to you for free and open access by Lehigh Preserve. It has been accepted for inclusion in Theses and Dissertations by an authorized administrator of Lehigh Preserve. For more information, please contact [preserve@lehigh.edu](mailto:preserve@lehigh.edu).

# Study of nanoparticle binding in a microfluidic platform

by Antony Thomas

A Thesis

Presented to the Graduate and Research Committee

of Lehigh University

in Candidacy for the Degree of

Master of Science

in

Bioengineering Program

Lehigh University

May-2012

© 2012 Copyright  
Antony Thomas

Thesis is accepted and approved in partial fulfillment of the requirements for the Master of Science in Bioengineering Program.

Study of nanoparticle binding in a microfluidic platform

Antony Thomas

---

Date Approved

---

Thesis Director

## ACKNOWLEDGMENTS

I would like to thank my advisor, Dr. Yaling Liu for his guidance and continuous support during my research work. The motivation he brought into the team helped in the progress of my work. He taught how rigorous persistence, along with smart research can bring out quality work. Without his encouragement this thesis would not have been possible.

The courses I took for the completion of 'Master's of Science' degree helped in strengthening my background in the biological and engineering aspects of research. I would like to thank all the professors and other faculty members who helped with the courses and shed new light into my research. Many thanks to my lab mates including but not limited to Jifu Tan, Shunqiang Wang, Abhijit Ramchandran and Qingjiang Guo. It was a pleasure working with you all.

Finally, I would like to express my deepest appreciation to my parents for helping me pursue my dream and being on my side through thick and thin. I would also like to thank my sister and brother-in-law for their support and love.

# TABLE OF CONTENTS

|  |           |
|--|-----------|
| <b>LIST OF FIGURES</b> .....   | <b>vi</b> |
| <b>Abstract</b> .....  | <b>1</b>  |
| <b>Chapter 1: INTRODUCTION</b> .....   | <b>2</b>  |
| <i>1.1 Background</i> .....  | 2         |
| 1.1.1 Microfluidics .....  | 2         |
| 1.1.2 Microfluidics in biology.....  | 3         |
| 1.1.3 Microfluidics in drug delivery.....  | 5         |
| 1.1.4 Proposed work in drug delivery .....   | 5         |
| <i>1.2 Characterization of NP delivery in microcirculation: the influence of blood cells and vascular geometry</i> ..... | 6         |
| 1.2.1 Targeted nano drug carriers in microcirculation .....  | 6         |
| 1.2.2 Current challenges in the study of drug delivery and distribution .....  | 6         |
| 1.2.3 Distribution of nano drug carriers under the influence of RBC .....  | 7         |
| 1.2.4 Influence of vessel geometry in nano drug carrier distribution.....  | 8         |
| <b>Chapter 2: Experimental methods</b> .....   | <b>10</b> |
| 2.1 Materials.....   | 10        |
| 2.2 Microfabrication.....  | 10        |
| 2.3 ICAM-1 modified PDMS Substrate .....   | 11        |
| 2.4 Anti-ICAM-1 coated micro/nano particles .....  | 12        |
| 2.5 Biodistribution test .....   | 12        |
| <b>Chapter: 3 Results and Discussion</b> .....   | <b>14</b> |
| 3.1 NP distribution across channel .....   | 15        |
| 3.2 100 nm particle binding distribution.....  | 16        |
| 3.3 3 $\mu\text{m}$ particle binding distribution.....   | 18        |
| 3.4 Mathematical modeling of particle binding .....  | 21        |
| 3.5 Influence of particle size on binding density .....  | 24        |
| 3.6 Influence of RBC on binding density of particles with different sizes .....  | 25        |
| <b>Chapter: 4 Conclusions</b> .....  | <b>28</b> |
| <b>Chapter: 5 Future Work</b> .....  | <b>30</b> |
| <b>References</b> .....  | <b>31</b> |
| <b>VITA</b> .....  | <b>37</b> |

## LIST OF FIGURES

- Fig. 1: (A) Auto CAD design of microchannel geometry, Inset illustrates the fabricated microfluidic chip during RBC-particle mixer testing; (B) The flow test set-up..... 11
- Fig. 2: Illustration of the steps involved in anti-ICAM-1 coating of PDMS surface. .... 12
- Fig. 3: (A) Fluorescent image of 100 nm particle flow at  $100 \text{ s}^{-1}$  shear rate in a  $20 \mu\text{m}$  channel; (B) Fluorescent intensity across channel width under pure 100 nm particle flow at  $100 \text{ s}^{-1}$  shear rate; (C) Fluorescent image of 100 nm particle flow with 40% RBCs at  $100 \text{ s}^{-1}$  shear rate in a  $20 \mu\text{m}$  channel; (D) Fluorescent intensity across channel width for 100 nm particle flow with 40% RBC at  $100 \text{ s}^{-1}$  shear rate. .... 15
- Fig. 4: Confocal fluorescence image showing distribution of anti-ICAM-1 coated 100 nm particles in a branched channel (top) and a straight channel (bottom) under different flow conditions and shear rates; (A)  $40 \text{ s}^{-1}$ , pure particle case; (B)  $40 \text{ s}^{-1}$ , effective concentration case; (C)  $40 \text{ s}^{-1}$ , RBC 40% case; (D)  $8 \text{ s}^{-1}$ , pure particle case; (E)  $8 \text{ s}^{-1}$ , effective concentration case; (F)  $8 \text{ s}^{-1}$ , RBC 40% case. (Scale bar:  $100 \mu\text{m}$ ) ..... 17
- Fig. 5: Particle binding density ( $\#/\mu\text{m}^2$ ) at shear rates between  $8\text{-}100 \text{ s}^{-1}$  under pure particle flow (red line), effective concentration flow (black dashed line) and RBC (40%) flow (blue dotted line); (A) 100 nm particles in straight channel; (B) 100 nm particles in branched channel..... 18
- Fig. 6: Confocal fluorescence image showing distribution of anti-ICAM-1 coated  $3 \mu\text{m}$  particles in branched channel (top) and straight channel (bottom) under different flow conditions and shear rates; (A)  $8 \text{ s}^{-1}$ , Pure particle case; (B)  $8 \text{ s}^{-1}$ , RBC 40% case; (C)  $100 \text{ s}^{-1}$ , Pure particle case; (D)  $100 \text{ s}^{-1}$ , RBC 40% case. (Scale bar:  $100 \mu\text{m}$ ) ..... 19
- Fig. 7: Particle binding density ( $\#/\mu\text{m}^2$ ) at shear rates between  $8\text{-}100 \text{ s}^{-1}$  under pure particle flow (red line) and RBC (40%) flow (blue dotted line) for  $3 \mu\text{m}$  particles in (A) straight channel and in (B) branched channel ..... 20
- Fig. 8: Particle binding density in analytical study at shear rates between  $8\text{-}100 \text{ s}^{-1}$  (black curve). Blue star represent particle binding density of 100 nm particles at pure particle flow in straight channel and red circles represent particle binding density of  $3 \mu\text{m}$  particles at pure particle flow in straight channel..... 23
- Fig. 9: Comparison of particle binding density ( $\#/\mu\text{m}^2$ ) in straight and branched channels for 100 nm particles and  $3 \mu\text{m}$  particles at shear rates between  $8\text{-}100 \text{ s}^{-1}$  for pure particle case. Inset graph shows ratio of 100 nm to  $3 \mu\text{m}$  particle binding density at shear rates between  $8\text{-}100 \text{ s}^{-1}$  for pure particle, straight channel case. .... 25
- Fig. 10: Comparison of particle binding density ( $\#/\mu\text{m}^2$ ) in straight and branched channel for 100nm and  $3 \mu\text{m}$  particles between  $8\text{-}100 \text{ s}^{-1}$  shear rates for RBC 40% case. Inset graph shows ratio of particle binding density in straight vs. branched channels for 100 nm (blue diamond markers) and  $3 \mu\text{m}$  (red square markers) particles at shear rates between  $8\text{-}100 \text{ s}^{-1}$  for RBC 40% case with trend lines..... 26

## Abstract

This work focuses on the characterization of nanoparticle (NP) delivery in microcirculation. In microvasculature network, the vessel size is comparable to that of red blood cells (RBCs) and the existence of blood cells largely influences the dispersion and binding distribution of NPs. The geometry of the microvasculature leads to non-uniform particle distribution and effects on the particle binding characteristics. We perform an *in vitro* study in a mimetic microfluidic chip, on the various factors that influence NP distribution and delivery such as vessel geometry, blood cells, particle size, and shear rates. RBCs are found to enhance the binding of NPs at all shear rates and for microparticles at higher shear rates. RBCs also interfere with the binding of microparticles at low shear rates. The NP binding density is around ten times higher when NPs flow along with 40% RBCs compared to the pure particle case. RBCs bring in an enhancement of two hundred fold in binding density for 3  $\mu\text{m}$  particle at high shear rates when compared to the pure particle case. Higher particle binding density is also observed at bifurcation region of the microvasculature geometry.



# Chapter 1: INTRODUCTION

## *1.1 Background*

### **1.1.1 Microfluidics**

Microfluidics is the characterization and manipulation of fluids on the nanoliter or picoliter scale in channels with dimensions of tens to hundreds of micrometres. The main advantages of applying microfluidic platforms are: use of very small quantities of samples and reagents, processing separations and detections with high resolution and sensitivity; low cost; short processing time and scaling down of size [1]. Most of the research in microfluidic systems are carried out on poly(dimethylsiloxane) (PDMS) [2-3]. PDMS is an optically transparent, soft elastomer. Ease of fabrication based on soft lithography allows new concepts to be easily incorporated in PDMS platform and tested [4]. This has made it a key material for exploratory research and research engineering at the early stages of development.

Currently, microfluidics platform has been applied in wide range of fields. In protein crystallization studies, microfluidic platform works as a sensor to screen conditions such as pH, ionic strength and composition, concentration etc. [5-6]. Other laboratory applications include high-throughput screening in drug development[7-8] mass spectroscopy coupled separations [9], bioanalyses[10], single cell or molecule examination and manipulation[11-14]. Microfluidic platforms has been used in the manipulation of multiphase flows, enabling the generation and manipulation of monodisperse bubbles[15-16] or droplets[17-18]. This feature has been applied in the production of polymer particles, emulsions and foams [19]. The microscale physics and

phenomena of microfluidic devices has been used to create systems that provide functionality useful to the life sciences. Macroscale systems has been brought down to the microfluidic "lab-on-a-chip" platform[20], an incorporation of multiple aspects of modern biology or chemistry labs on a single microchip.

### **1.1.2 Microfluidics in biology**

Biological systems are complex which makes accurate and precise experimentation to be a cumbersome task. Most biological experimentation focuses on highly detailed patterns in the micron level, which lacks the throughput necessary to reconstruct the entire biological system. High-throughput testing platform often lacks the fidelity and detail necessary to fully comprehend the micron scale mechanisms. Recent advances in the bio and nano technologies have led to the development of novel, biological microsystem platforms for application and analysis in the field of life science. These microsystems provide an opportunity to comprehend studies in detail and high-throughput analysis is possible by massively arraying devices on a chip [21]. These new platforms have revolutionized the way we do science and have led to the development of a number of ultrasensitive bio-analytical devices.

Microfluidic lab-on-a-chip devices have found application in a number of diverse areas such as pollution monitoring, clinical diagnostics, drug discovery and biohazard detection. High-resolution and localized application of experimental conditions in biomimetic physiological conditions, practically promotes the implementation of the system in all possible directions.

Standard laboratory analyses such as, sample purification, labeling, detection and separation have been performed automatically in microfluidic platform as the sample is moved via microchannels to different regions of a chip. On-chip cell detection and handling techniques like cell culture devices, microfabricated flow cytometers, cell sorting devices etc. have also been possible on microfluidic platforms. Microfabricated cell culture devices have made possible the analysis of drug effects, osmotic balance, cytogenic and immunologic responses and metabolism in an *in vitro* set up [7]. Recently even culture of stem cells have been performed on these platforms [22]. Optical tweezer based capture of beads, cells and deoxy ribo nucleic acid (DNA) has been performed on microfluidic devices [23]. Devices capable of performing high-throughput analysis of the electrical properties of single cells and other organisms have also been developed [24]. High-speed analysis and sorting of individual cells and polymer beads based on their optical properties are also available on the microfluidic platform [25-26].

On-chip separation techniques for subcellular components such as proteins and DNA have found wide application in the area of micro total analysis systems [27-29]. Different variants of the standard enzyme-linked immunosorbent assay have been demonstrated on microfluidic chip. On-chip examples include the detection of HIV-1 from infected and non-infected patients[30], the detection of cytokine tumor necrosis factor  $\alpha$  with picomolar sensitivity[31], the integration of standard immunostrip into microflow channels for the detection of cardiac troponin I[32] and the use of microfabricated filters for bead-based detection of viruses [33].

### **1.1.3 Microfluidics in drug delivery**

The ability of microfluidic technology to miniaturize assays and increase experimental throughput have generated significant interest in the drug discovery and development domain. It has been applied in different stages of the process, including target selection, lead identification, preclinical tests, clinical trials, chemical synthesis, formulations studies and product management [34-35]. Much of drug discovery and applications are based on the selective binding of low molecular weight molecules to bioactive macromolecules [36]. Typically, these ligand-binding studies are performed by exposing the target to various concentrations of a compound. Microfluidic devices have been used for ligand-binding studies to minimize interaction times, improve sensitivity and increase throughput.

### **1.1.4 Proposed work in drug delivery**

In this thesis an evaluation on the distribution and adhesion of drug carrier particles in an *in vitro* biomimetic microfluidic platform is performed. The distribution of particles in the nano and micron range is studied under different physiologically relevant shear rates in channels that mimic microvasculature. The channels are coated with biomolecules that are overexpressed by the endothelial cell layer of diseased microvasculature. In this way, the channels of the microfluidic device exhibit conditions similar to *in vivo*. Particles mimicking drug carriers are coated with ligands having affinity to these biomolecule coated in the channels and are flown through them.

One of the primary modes of applying drug particles is through blood vessels. Therefore, RBCs and the blood vessel geometry can influence the particle transport

characteristics. Our work also studies the effect of RBCs on particle distribution and binding dynamics. The microchannels also incorporate straight and bifurcating features present in typical microvasculature network.

## ***1.2 Characterization of NP delivery in microcirculation: the influence of blood cells and vascular geometry***

### **1.2.1 Targeted nano drug carriers in microcirculation**

Various techniques in NP targeted drug delivery have been developed in recent years to reduce side effects, toxicity, and lower drug dosage [37]. The use of NPs in drug delivery help in targeted delivery and release of drugs at disease region, serving the dual role of diagnosis and therapy [38]. The drug uptake efficacy of NP based drug carriers is higher compared to the larger particle carriers which are easily cleared off by the human mononuclear phagocyte system. NPs also have larger surface to volume ratio[39], which helps attachment of multiple functional groups and thereby enhance targeting. Nano drug based delivery systems has great potential to achieve efficient targeting of cells and molecules in inflammation and cancer conditions [40].

### **1.2.2 Current challenges in the study of drug delivery and distribution**

Recent theoretical modeling works demonstrate a decrease in NP adhesion probability with an increase in local blood flow rate [41]. Due to bioethical regulations and complex physiological conditions, it is very challenging to quantify the NP delivery process *in vivo*. Most of the current studies are carried out *in vitro* by flowing NP buffer

solutions in flow chambers or channels [42-43]. However, the result from these studies are applicable to large blood vessels but not to microvasculature. Microvasculature refers to part of the circulatory system consisting of capillaries, arterioles, and venules [44]. Microvasculature parameters such as vascular geometry, target receptors expression level and flow shear rate, must be considered while performing these studies *in vitro*. Study on specific receptor mediated binding of nano drug carriers under various physiologically relevant conditions help in understanding parameters that allow enhanced targeted delivery and also determine the actual bioavailability of drugs. This work also addresses the current challenge of quantifying NP binding density at specific vascular locations, which is critical for clinical drug dosage control.

### **1.2.3 Distribution of nano drug carriers under the influence of RBC**

Relevant works on characterization of NP delivery assumes NPs in a buffer suspension without considering RBCs [42, 45]. Blood is a complex bio-fluid consisting of RBCs, monocytes, platelets, proteins etc. Blood flow in microvasculature is a two-phase phenomenon as the vessel diameter becomes comparable to the size of RBCs. *In vitro* studies on RBC mediated particle delivery has to consider various *in vivo* microvasculature parameters, such as Fåhræus–Lindqvist effect [46], Segre–Silberberg effect [47-48], cell-free-layer (CFL) formation [49-51], vessel bifurcations [52] and blunt velocity profile [53-56].

When flowing along with RBCs, their shape, size and concentration can induce movements not available in homogenous fluids [57-59]. RBCs under shear flow can form small regions of convection under its rotating and colliding movement. This can give way

to apparent raise in diffusion coefficient for particles in flow along with RBCs. The targeted binding of nano drug carriers to diseased cells requires the NPs to marginate toward the vascular wall. RBCs tend to flow in the core region of blood stream thereby dispersing out the NPs to the nearby wall region. This phenomenon largely influences NP distribution and binding dynamics. In this work, we will consider the influence of RBCs on NP distribution and binding under different vascular shear rates and geometries.

#### **1.2.4 Influence of vessel geometry in nano drug carrier distribution**

Vascular geometry is another factor that has not been well studied in NP delivery process. Blood circulatory system consists of large blood vessels like the arteries and veins (~15-0.5 mm), smaller vessels like the arterioles, venules (100-500  $\mu\text{m}$ ) and capillaries (~10  $\mu\text{m}$ ). The distribution of drug particles in real vascular network having hierarchical geometry will depend on local shear rate, flow velocity, pressure and volume [60]. Our study considers the distribution of nano and micron sized particles in a branching channel that mimics the geometry and flow conditions of a complex vasculature network. Also a comparison of particle binding density between the bifurcating channel and the straight channel is performed to examine the effect of non-uniform distribution of particles at vessel bifurcations with and without RBCs.

The specificity of targeting is brought about by applying ligand-receptor chemistry in our microfluidic platform. The biomimetic chip is coated with intercellular adhesion molecule 1 (ICAM-1) protein, a cell-surface glycoprotein member of the Ig super-family. Under inflammatory conditions, interaction between endothelial cells and blood constituents occur by the up-regulation of intercellular adhesion molecules such as

ICAM-1 on the surface of endothelial cells and leukocyte [61-62]. This mediates the targeted migration of leukocytes into specific areas of inflammation [63]. Various ICAM-1 based therapeutic agents for cancer immunotherapy and other modes of treatment are used nowadays [64-65]. ICAM-1 is also not known to produce any conformational change under shear like von Willebrand Factor that might affect the binding behavior of particles. Anti-ICAM-1 coated 100 nm particles are used as a model system to study the influence of RBCs and vascular geometry on NP delivery. A comparative study is performed with 3  $\mu\text{m}$  particles and to study how particle size influences the binding characteristic.

In the following sections, methods applied to modify the microfluidic platform are discussed along with various testing conditions. The results and discussion section addresses the binding characteristics of 100 nm and 3  $\mu\text{m}$  particles. The influence of particle size in binding is analyzed next followed by the influence of RBCs. Finally, the conclusion and future work are presented.



## **Chapter 2: Experimental methods**

### ***2.1 Materials***

Human ICAM-1/CD54 FITC MAb (Clone BBIG-I1) Mouse IgG1, ICAM-1/human IgG1 Fc chimera (R&D Systems, Minneapolis, MN), protein G (Biovision, Milpitas, CA), fluorescent red latex 100 nm particles, bovine serum albumin (BSA), 3-aminopropyltrimethoxysilane (Sigma Aldrich, St Louis, MO), 3  $\mu\text{m}$  particles (Spherotech, Lake Forest, IL), Polydimethylsiloxane (Dow Corning, Midland MI), single donor human whole blood (Innovative Research), tygon tubing, syringe, needles.

### ***2.2 Microfabrication***

The required microfluidic design is photo-lithographically patterned on a silicon wafer using SU-8 2050 photoresist. Microfluidic devices are fabricated using Sylgard 184 PDMS. PDMS base is mixed with its cure at 1:10 (v/v) ratio following the basic techniques in soft lithography[66]. The PDMS mixture is poured on the silicon wafer, which acts as the master template. The hard PDMS layer is peeled out after baking and the features are inspected. The microfluidic device is made by binding the PDMS pattern on a clean glass slide after exposing them to oxygen ( $\text{O}_2$ ) plasma. The flow channels are 100 microns ( $\mu\text{m}$ ) wide and 40  $\mu\text{m}$  in height. Both straight and bifurcating features are included in the design.

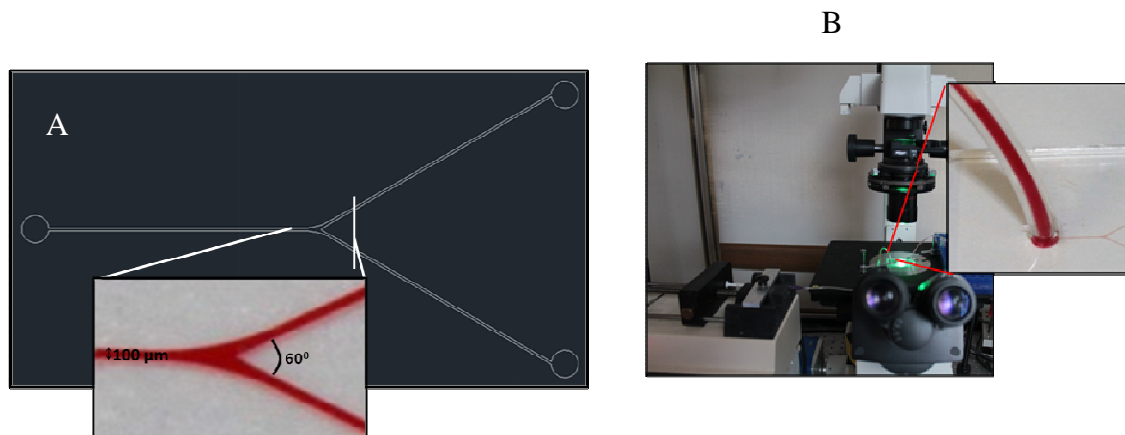


**Fig. 1:** (A) Auto CAD design of microchannel geometry, Inset illustrates the fabricated microfluidic chip during RBC-particle mixer testing; (B) The flow test set-up.

### ***2.3 ICAM-1 modified PDMS Substrate***

After binding with glass, the PDMS devices were silanized with 3-aminopropyltrimethoxysilane to improve protein adsorption. Unbound silane molecules were removed by washing the device with an adsorption buffer (0.1M NaHCO<sub>3</sub>, pH 9.2). Then the devices were incubated for 2 hrs at room temperature with saturating concentration of protein G in adsorption buffer (100 μg/ml). ICAM-1 Fc chimera protein solution in PBS (100 nM) was introduced after washing the substrates three times with PBS to remove any excess protein G. The devices were incubated with ICAM-1 for 1 hr at room temperature [42]. The microfluidic chips were purged with 1% BSA containing 0.05% Tween20 one hour prior to testing. Devices were flushed with PBS to remove any unbound BSA before testing.

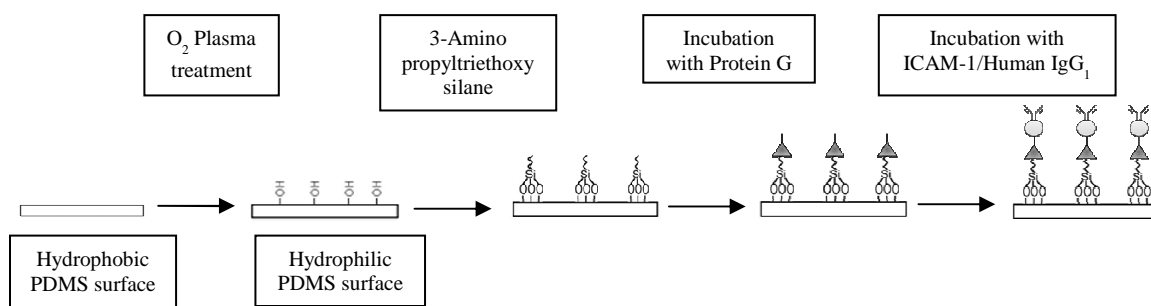


**Fig. 2:** Illustration of the steps involved in anti-ICAM-1 coating of PDMS surface.

## 2.4 Anti-ICAM-1 coated micro/nano particles

Anti-ICAM-1 protein is passively adsorbed on the 3  $\mu\text{m}$  and 100 nm fluorescent polystyrene particles as previously described [67-69]. The particles were incubated overnight in anti-ICAM-1 solution (100 mg/ml). The antibody and particles were mixed in a suitable buffer and placed in an orbital shaker at room temperature. The particles were used immediately after three washes to ensure the complete removal of free or unbound proteins. The Fc (Fragment, crystallizable) portion of the ICAM-1 antibody is more hydrophobic and gets adsorbed on the polystyrene surface than the antigen binding region, providing a biologically active orientation. BSA coated particles were used as negative control. Flow cytometry based analysis was performed on the particles to evaluate protein coating.

## 2.5 Biodistribution test

Anti ICAM-1 coated particles were flown through ICAM-1 modified microfluidic devices at different shear rates between 8 to 100  $\text{s}^{-1}$ . This corresponds to physiologically relevant values observed in the microvessels [70-74]. The flux rate is kept constant at

1012 and  $5 \times 10^9$  for 100 nm and 3  $\mu\text{m}$  particle case respectively. Fluid flow was brought about using a programmable syringe pump (Harvard Apparatus). The fluid flow rate controls the volumetric flow rate which is proportional to the wall shear rate. The wall shear rate  $\dot{\gamma}_w$  was derived from the volumetric flow rate  $Q$  using the following relation [42]:

$$\dot{\gamma}_w = 6Q/H^2W$$

'H' is the height and 'W' is the width of the microfluidic device.

Each flow test case was run for 10 min and the microfluidic chips were washed with PBS for clearing any unbound particles in the 100 nm case. The biodistribution of NPs were analyzed on a high resolution laser confocal fluorescence microscope (FV1000-IX81, Olympus). Washing out unbound 3  $\mu\text{m}$  particles posed higher probability of detachment due to external influences. Here the flow set up was assembled on the stage of an inverted fluorescence microscope and after 10 min of flow, the imaging was performed keeping the exposure time low. Only the bonded 3  $\mu\text{m}$  fluorescent particles were captured by the cooled CCD camera device, while the free flowing ones appeared blurred.

## Chapter: 3 Results and Discussion

The microfluidic device is designed to mimic the geometry of a typical microvasculature. The design contains both straight and branching channels. In our study, the tests are carried out on a range of wall shear rates between 8 to 100  $\text{s}^{-1}$ . The particle flux is kept constant based on the shear rate to make sure the total number of particles flown through each device is same for all the cases. This represents a constant drug dosage in clinical setup.

Three testing conditions are carried out in this work: particles in pure buffer, particle mixed with 40% RBC (hematocrit percentage) and particle mixed with diluted RBC to reach the same effective concentration as pure particle case. The effective concentration case has the same available free space for particles as compared with pure particle case even though RBCs are added to the suspension. The latter two cases help in studying the influence of RBCs on particle diffusion process and binding dynamics. RBCs have a biconcave shape of  $\sim 8 \mu\text{m}$  diameter and  $\sim 2 \mu\text{m}$  thickness, and is highly deformable [51, 75]. In microvessels the flexible RBCs migrate radially towards the center region based on different hemorheology factors such as shear rate, viscosity, hematocrit concentration, RBC aggregation and deformability. This result in a RBC concentrated core region and a cell-free plasma layer near the vascular wall called cell free layer (CFL) [49, 75-76].

### 3.1 NP distribution across channel

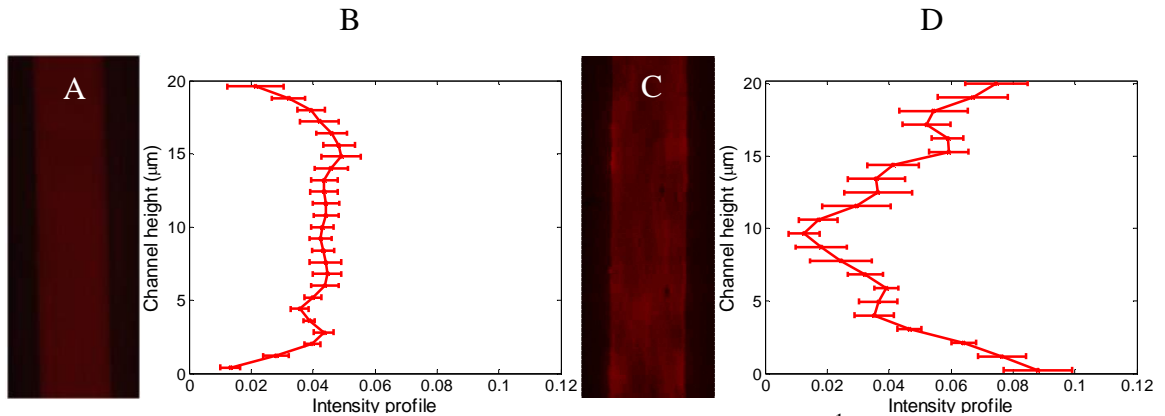


**Fig. 3:** (A) Fluorescent image of 100 nm particle flow at  $100 \text{ s}^{-1}$  shear rate in a  $20 \mu\text{m}$  channel; (B) Fluorescent intensity across channel width under pure 100 nm particle flow at  $100 \text{ s}^{-1}$  shear rate; (C) Fluorescent image of 100 nm particle flow with 40% RBCs at  $100 \text{ s}^{-1}$  shear rate in a  $20 \mu\text{m}$  channel; (D) Fluorescent intensity across channel width for 100 nm particle flow with 40% RBC at  $100 \text{ s}^{-1}$  shear rate.

To find out the distribution of NPs in a microchannel during flow, fluorescent 100 nm particles were flown through a  $20 \mu\text{m}$  channel at a shear rate of  $100 \text{ s}^{-1}$ . Fluorescence intensity based distribution of NPs in the channel was analyzed. Fig. 3A and 3C shows 100 nm particle distributions at pure particle and RBC 40% case respectively. The fluorescence intensity distribution in pure particle case (Fig. 3B) shows uniform particle distribution along the channel width.

The RBC 40% case (Fig. 3D) shows an interesting non-uniform distribution of NPs in blood flow, with peaks coincident with the CFL. A high intensity of 0.08 is observed near to the wall region and in the core region the intensity decreases to 0.01. Such non-uniform distribution indicates that RBCs tend to migrate towards the core region during flow which leads to the margination of NPs to the near wall CFL region, leading to higher fluorescence intensity. Such high NP concentration near the CFL results in higher binding rate, which is presented in the following sections.

### ***3.2 100 nm particle binding distribution***

The 100 nm particles show an increase in particle binding density at decreased shear rates. Fig 4 shows confocal scanning fluorescence image of particle binding distribution for the  $40 \text{ s}^{-1}$  and the  $8 \text{ s}^{-1}$  shear rates. The particle binding density for RBC 40% case is higher compared to the pure particle case (Fig. 4C compared to 4A and Fig. 4F compared to 4D). The effective concentration case also shows enhanced binding compared to the pure particle case (Fig. 4B compared to Fig. 4A and Fig. 4E compared to Fig. 4D).

To quantify and characterize the influence of RBC and channel geometry on NP binding, we measure the binding density by counting individual bonded particles through image processing. The particle binding density is calculated based on the number of particles bonded per unit area ( $\#/\mu\text{m}^2$ ). Fig. 5 compares the particle binding density for straight and branched channel cases. Both show a decrease in binding density of NPs with increased shear rates. The binding of receptor coated particles flowing in ligand modified surface is governed by the shear rate of flow. At high shear rates, there is less probability for binding to take place leading to a fall in particle binding density. Shear rate determines the critical time available for adhesive receptor/ligand organization and thereby cross-linking leading towards binding [77]. The mean contact time for bond formation between a receptor/ligand pair decreases with increase in shear rate, thereby decreasing the efficiency of bond formation. At lower shear rates the NPs have longer time period to process multivalent bond formation process under the complex dynamic flow condition. This leads to higher particle binding density at lower shear rates and decrease in particle binding density with an increase in shear rate [68].

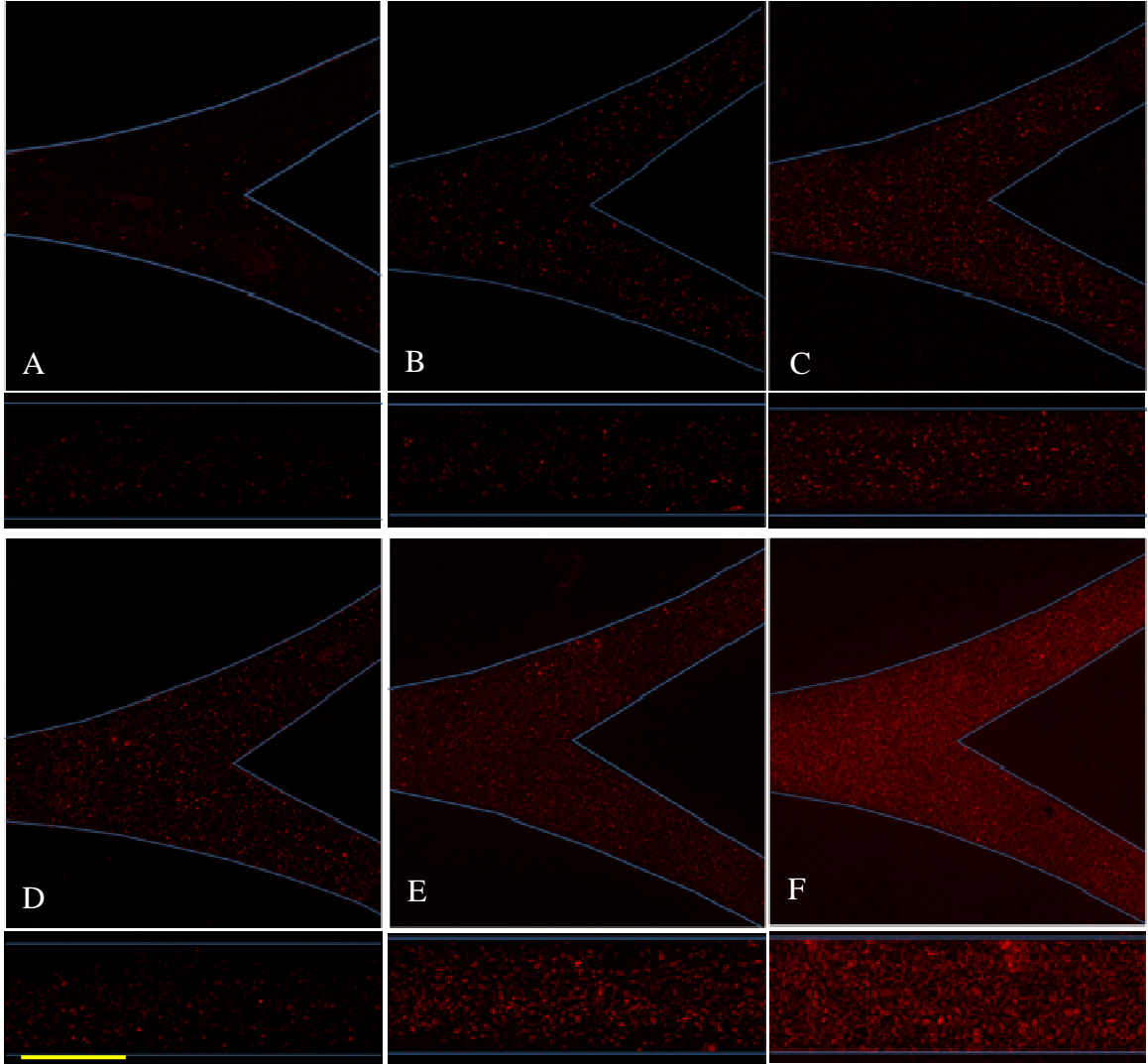


**Fig. 4:** Confocal fluorescence image showing distribution of anti-ICAM-1 coated 100 nm particles in a branched channel (top) and a straight channel (bottom) under different flow conditions and shear rates; (A)  $40 \text{ s}^{-1}$ , pure particle case; (B)  $40 \text{ s}^{-1}$ , effective concentration case; (C)  $40 \text{ s}^{-1}$ , RBC 40% case; (D)  $8 \text{ s}^{-1}$ , pure particle case; (E)  $8 \text{ s}^{-1}$ , effective concentration case; (F)  $8 \text{ s}^{-1}$ , RBC 40% case. (Scale bar:  $100 \mu\text{m}$ )

The RBC 40% case exhibits around 10 times higher binding density compared to that of pure NPs flow. This enhanced binding is induced by the axial-migration and tumbling motion of RBCs undergoing deformation, which leads to the exclusion of NPs from the center region to the CFL [51, 75]. This increase in NP density near the wall region leads to more frequent interaction between the anti-ICAM-1 coated NPs and the



ICAM-1 coated wall surface, thus higher probability for binding. The particle binding density increases around 2.5 times in the effective concentration case compared to the pure particle flow. This indicates that the enhanced NP binding in the RBC 40% case is not just because of volume exclusion, but a combined effect along with the migration of particles towards the near wall CFL region.

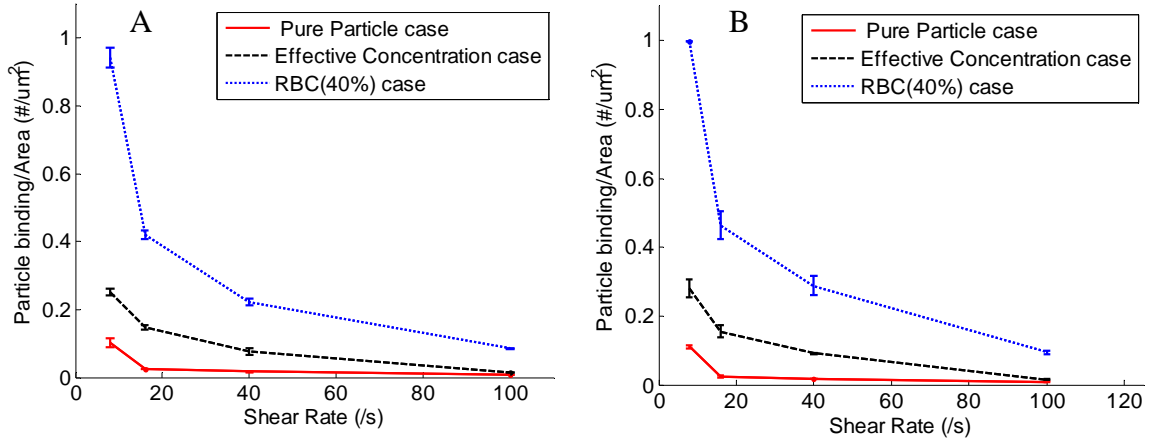


**Fig. 5:** Particle binding density ( $\#/\mu\text{m}^2$ ) at shear rates between  $8\text{--}100\text{ s}^{-1}$  under pure particle flow (red line), effective concentration flow (black dashed line) and RBC (40%) flow (blue dotted line) for 100 nm particles in; (A) straight channel; (B) branched channel

### 3.3 $3\text{ }\mu\text{m}$ particle binding distribution

To explore whether the observed NP binding pattern under different flow condition apply to microparticles, tests were carried out on  $3\text{ }\mu\text{m}$  particles which is similar to the size of platelets.

Confocal fluorescence images of anti ICAM-1 coated  $3\text{ }\mu\text{m}$  particle distribution on ICAM-1 modified straight and branched channels are shown in Fig 6. Particle distribution at  $8\text{ s}^{-1}$  shear rate for pure particle case and RBC 40% case are shown in Fig 6A and Fig. 6B respectively. Similarly, Fig. 6C and Fig. 6D show particle binding distribution for pure particle case and RBC 40% case at  $100\text{ s}^{-1}$  shear rate respectively

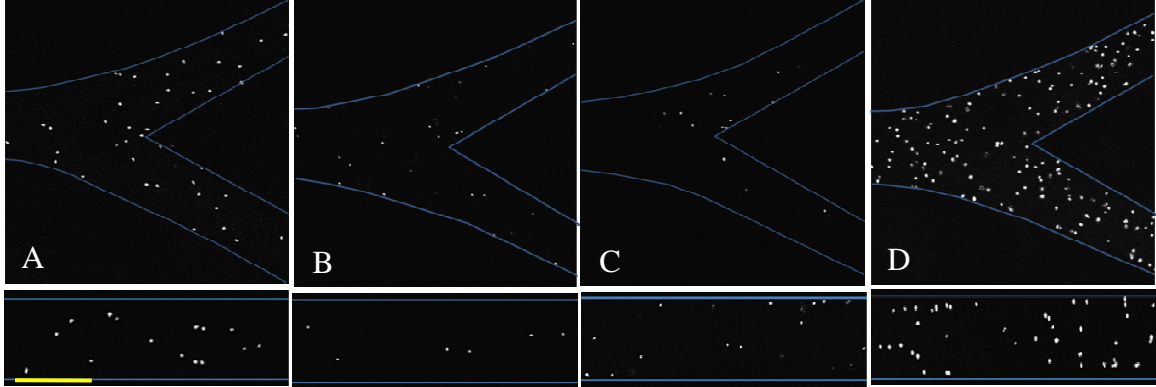


**Fig. 6:** Confocal fluorescence image showing distribution of anti-ICAM-1 coated 3  $\mu\text{m}$  particles in branched channel (top) and straight channel (bottom) under different flow conditions and shear rates; (A)  $8\text{ s}^{-1}$ , Pure particle case; (B)  $8\text{ s}^{-1}$ , RBC 40% case; (C)  $100\text{ s}^{-1}$ , Pure particle case; (D)  $100\text{ s}^{-1}$ , RBC 40% case. (Scale bar: 100  $\mu\text{m}$ )

In Fig. 7, the 3  $\mu\text{m}$  particle binding densities in a straight and a branched channel are compared. To compare with the 100 nm case, the binding density of 3  $\mu\text{m}$  particles have been normalized to reach the same scale as 100 nm particles as the particle flux used were different. The pure particle case shows decrease in particle binding density with increase in shear rate for both straight and branched channel cases. Similar results have been observed in other studies [78] and in our 100 nm particle binding study (Fig. 5).

However, for the RBC 40% case, an increase in particle binding density is observed with increased shear rate. This is contradictory to what is observed in the NP case. At lower shear rates, RBCs interfere with the attachment or promotes the detachment of attached microparticles. This might be induced by the brushing/colliding of RBCs against the bonded microparticles as they flow much closer to the vessel wall at low shear rates. With a decrease in shear rate, the CFL thickness reduces because the RBCs have a reduced tendency to migrate towards the center and the flow also has a blunt velocity profile [76, 79-80] [49]. This would allow these RBCs to brush against the

attached microparticles and thus detach them from the ICAM-1 coated surface. Such phenomenon is not observed under high shear flow conditions [68]. At higher shear rate, a wider CFL reduces the interaction between the flowing RBCs and bonded microparticles and explains the increase in microparticle binding. Similar enhanced concentration near the wall region and binding at shear rates above  $50\text{s}^{-1}$  is observed for platelets [81-84].

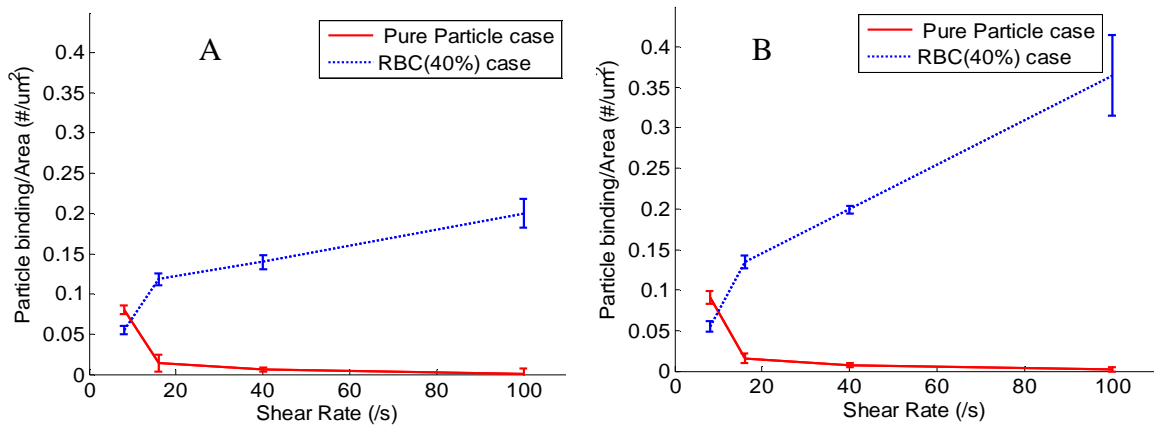


**Fig. 7:** Particle binding density ( $\#/\mu\text{m}^2$ ) at shear rates between  $8\text{-}100\text{ s}^{-1}$  under pure particle flow (red line) and RBC (40%) flow (blue dotted line) for  $3\text{ }\mu\text{m}$  particles in (A) straight channel and in (B) branched channel

Compared to the pure particle case, almost an increase of 200 fold is observed in binding density for the RBC 40% flow case at high shear rates. Here, a size based exclusion effect increases the margination of  $3\text{ }\mu\text{m}$  particles to the near wall CFL region from the RBC concentrated core region as seen in previous works[85-86]. This effectively increases the concentration of  $3\text{ }\mu\text{m}$  particles in the near wall CFL region. Thus the particles are confined in between the channel walls and the RBC concentrated core region and being in this transport limited region, the interaction between the RBCs and targeted particles increases the collision between the anti-ICAM-1 coated particles

with the ICAM-1 coated PDMS surface. This phenomenon have been observed and explained in other works [86-87]. This excess RBC generated force on the particles helps them in overcoming the disruptive forces generated by increased shear rate and thus helps in binding. This increases the particle binding density for 3  $\mu\text{m}$  particles at high shear rates.

Comparatively, only a smaller percentage of 100 nm particles marginate to the near wall region [88] while most of them still tend to flow along with RBCs in the core region because of their smaller size. This along with their smaller size compared to the CFL (2-20  $\mu\text{m}$  [89]) reduces their interaction with the RBC core and thereby produces lesser increase in particle binding density compared to the 3  $\mu\text{m}$  particle case.

A study on diffusivity of platelets on channels comparable to microvasculature found RBCs increase the range of diffusivity 50 to 250 times depending on hematocrit concentration and shear rate applied [90]. Our results follow similar trend with microparticles being of size comparable to that of platelets.

### ***3.4 Mathematical modeling of particle binding***

The particle binding density data for 100 nm and 3  $\mu\text{m}$  particles based on shear rate shows a non linear drop over shear rate. This is observed for all the three test cases in the 100 nm particle flow case and pure particle flow case for the 3  $\mu\text{m}$  particles. The only exception is the 40% RBC, 3  $\mu\text{m}$  particles case as its particle binding characteristics are heavily influenced by RBCs. In order to understand the effect of shear rate in particle binding density, a mathematical model is introduced.

An analytical model is proposed for the relationship between shear rate and particle binding density. The number of particles in an annular region within the distance reachable by diffusion can be estimated as:

$$N_{density} = \frac{\# \text{ of binding NPs}}{A} = \frac{cV}{A} = \frac{cdA}{A} = cd$$

Where  $A$  stands for the binding area,  $d$  stands for the average distance induced by Brownian motion,  $c$  stands for the concentration and  $V$  stands for the volume within which particles could be bound.  $N_{density}$  stands for particle binding density. Here, the distance induced by Brownian motion could be calculated as following:

$$d = \sqrt{2Dt}$$

Where  $D$  stands for diffusion coefficient of particles.

The time  $t$  could be calculated as.

$$t = \frac{l}{v} = \left( \frac{l}{\dot{\gamma}d} \right)$$

So substitution yields:

$$d = \left[ \frac{(2Dl)}{\dot{\gamma}} \right]^{1/3}$$

In consideration of the concentration  $c$ , based on the particle number conservation, we have:  $cA_0\tilde{v}t = \phi A_0t \rightarrow c = \frac{\phi}{\tilde{v}} = \frac{\phi A_0}{Q}$

Where  $A_0$  is the crossing area of the channel,  $\tilde{v}$  is the average velocity,  $t$  is the flowing time and  $\phi$  is the particle flux which is constant in our experimental case.  $Q$  is the flow rate which could be expressed as:  $\dot{\gamma}w = 6Q/H^2W$

Where  $H$  is the height of the channel and  $w$  is the width of channel. So substitution yields:  $C = \frac{6\phi A_0}{H^2 w \dot{\gamma}} = \frac{6\phi}{H \dot{\gamma}}$

Hence, we could attain the relationship between particle binding density and shear rate as:

$$N_{density} = \frac{6\phi}{H\dot{\gamma}} \cdot \left(\frac{2Dl}{\dot{\gamma}}\right)^{1/3} = \frac{6 \cdot (2Dl)^{1/3} \phi}{H\dot{\gamma}^{4/3}}$$

Following this relationship we analytically attain the relationship between particle binding density at different shear rates, as shown in Fig. 8.

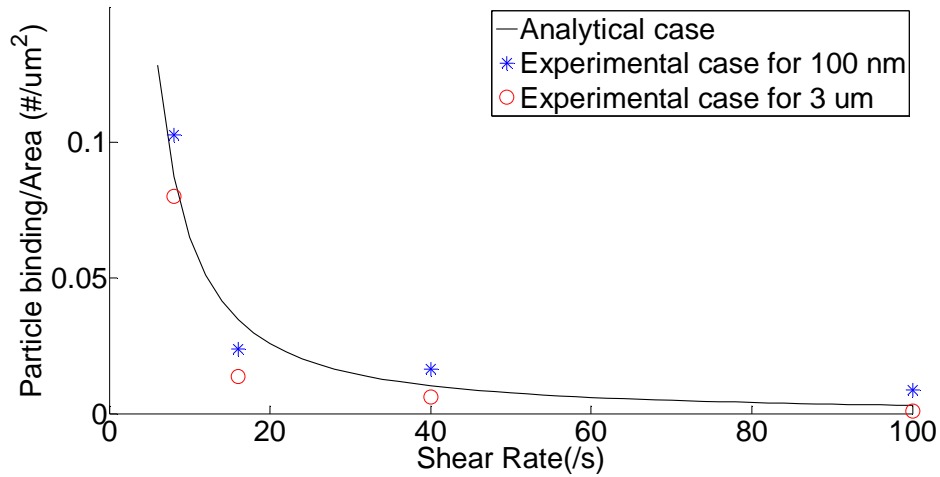


**Fig. 8:** Particle binding density in analytical study at shear rates between 8-100 s<sup>-1</sup> (black curve). Blue star represent particle binding density of 100 nm particles at pure particle flow in straight channel and red circles represent particle binding density of 3 μm particles at pure particle flow in straight channel.

In Fig. 8, the black curve represents the particle binding density from the analytical solution. A significant fall in particle binding density is observed between shear rates of 8-16  $s^{-1}$ . This validates the role played by shear rate in the erratic drop in particle binding density observed for the 100 nm (blue stars) and 3  $\mu m$  (red circles) particles cases at lower shear rates in the experimental work. We compare the particle binding density found experimentally for 100 nm particles and 3  $\mu m$  particles in the pure particle flow case in straight channel to the trend seen in analytical work. Both cases follow similar trend. In the experimental work, the flow cases with RBCs exhibit similar trend in binding, though RBCs tend to amplify the particle binding density.

### ***3.5 Influence of particle size on binding density***

Fig. 9 compares the binding density in straight and branched channels for 100 nm and 3  $\mu m$  particles at shear rates between 8-100  $s^{-1}$  for pure particle case. The 100 nm particles show higher particle binding density compared to the 3  $\mu m$  ones and the binding density decreases with increased shear rate. The ratio of particle binding density between 100 nm and 3  $\mu m$  particles increases with shear rate (inset graph). About 9 fold higher particle binding density is observed for 100 nm particles compared to 3  $\mu m$  particles at 100  $s^{-1}$  shear rate. This decrease in particle binding with an increase in particle size is consistent with that reported in literature [91] especially at higher shear rates [92]. With an increase in shear rate, the disruptive force and torque acting on a 3  $\mu m$  particle is larger compared to smaller 100 nm particles [93]. The binding of particles to a surface depends on the balancing of disruptive force from shear flow and adhesive force from the receptor ligand bonds. Particles of bigger size has reduced binding and in our study the

increase in shear rate reduces the binding of 3  $\mu\text{m}$  particles. As explained before, the 100 nm particles diffuse more to the wall region compared the 3  $\mu\text{m}$  particles based on particle size. This also promotes better NP binding for pure particle case. A slightly higher binding density is found for both 100 nm and 3  $\mu\text{m}$  particles in branching channels compared to straight channels.

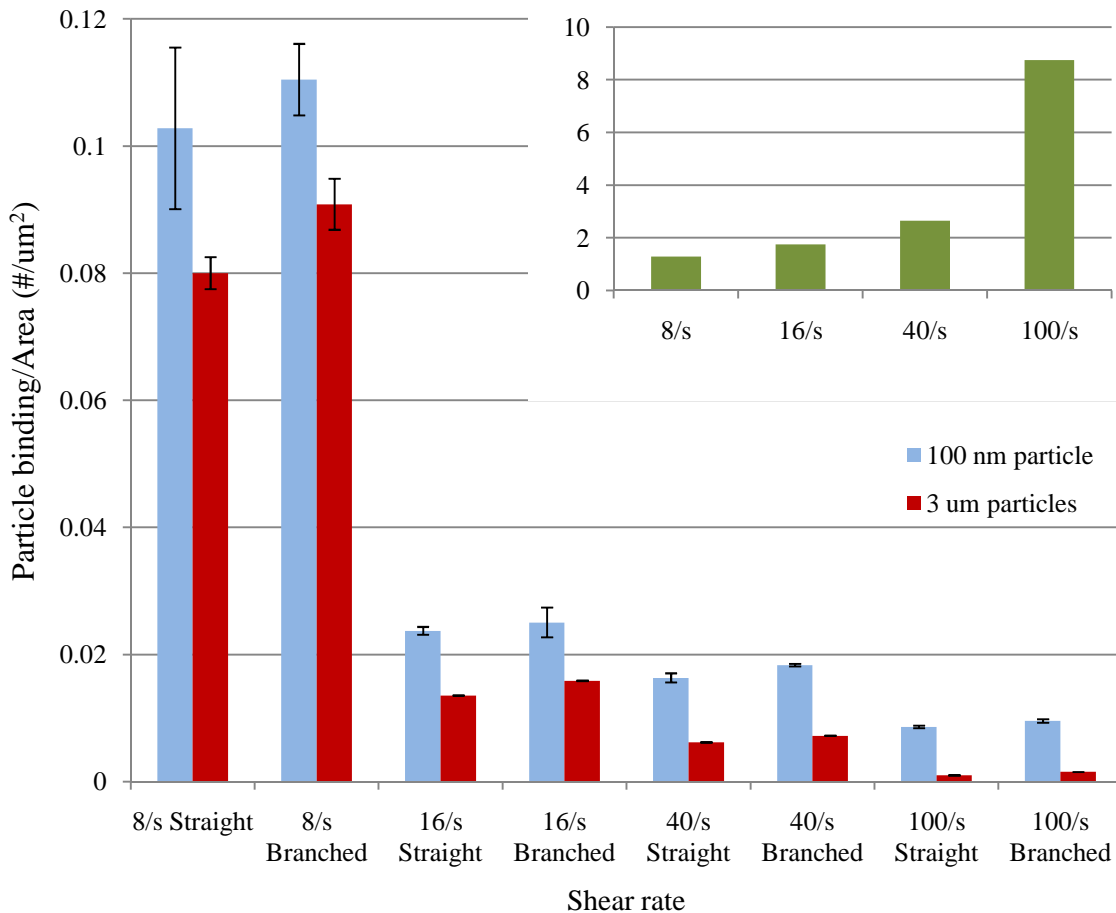


**Fig. 9:** Comparison of particle binding density ( $\#/\mu\text{m}^2$ ) in straight and branched channels for 100 nm particles and 3  $\mu\text{m}$  particles at shear rates between 8-100  $\text{s}^{-1}$  for pure particle case. Inset graph shows ratio of 100 nm to 3  $\mu\text{m}$  particle binding density at shear rates between 8-100  $\text{s}^{-1}$  for pure particle, straight channel case.

### 3.6 Influence of RBC on binding density of particles with different sizes

The influence of RBCs on particle binding varies according to particle size. Fig. 10 compares the particle binding density in straight and branched channels for 100nm



and 3  $\mu\text{m}$  particles between 8-100  $\text{s}^{-1}$  shear rates for the RBC 40% case. As explained before, the particle binding density for 100 nm particles decrease with shear rate, while for the 3  $\mu\text{m}$  particles the binding density increase with shear rate. The inset graph in Fig. 10 compares the ratio of particle binding density in branched versus straight channels at different shear rates for both particle sizes.

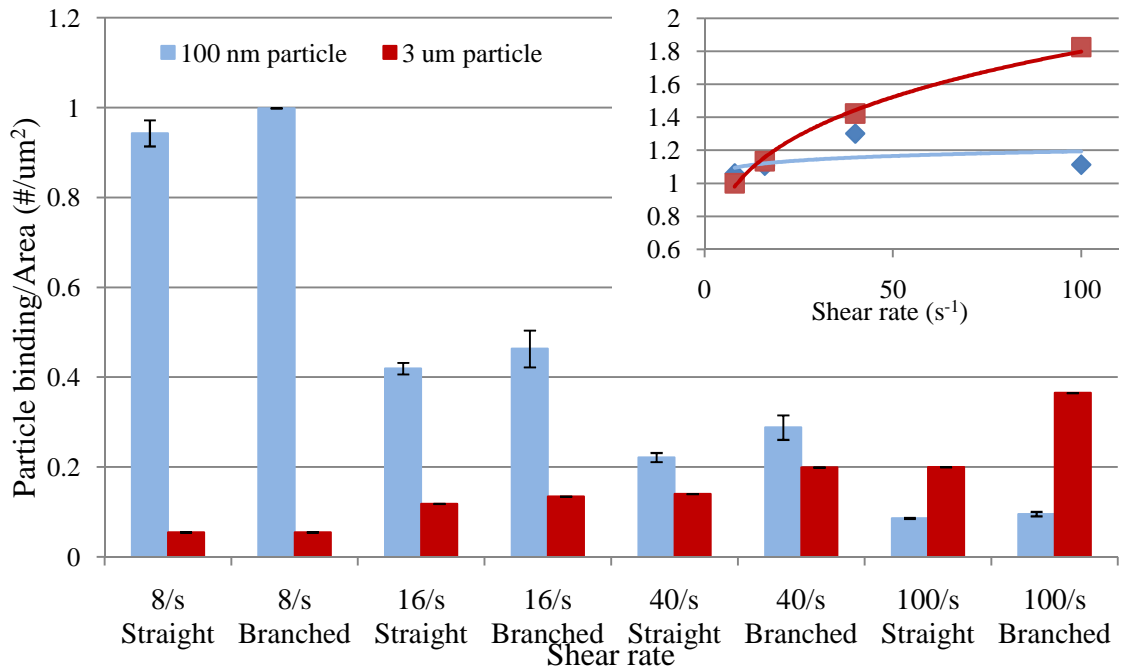


**Fig. 10:** Comparison of particle binding density ( $\#/\mu\text{m}^2$ ) in straight and branched channel for 100nm and 3  $\mu\text{m}$  particles between 8-100  $\text{s}^{-1}$  shear rates for RBC 40% case. Inset graph shows ratio of particle binding density in straight vs. branched channels for 100 nm (blue diamond markers) and 3  $\mu\text{m}$  (red square markers) particles at shear rates between 8-100  $\text{s}^{-1}$  for RBC 40% case with trend lines.

For the 3  $\mu\text{m}$  particles, an increase in particle binding density is observed at the branching channels compared to the straight channels with increased shear rate (ratio increases from 1 to ~1.8). No significant difference in particle binding density between branched and straight channels was observed for the 3  $\mu\text{m}$  particles in the pure particle case. There is also no significant difference in binding density for the 100 nm particles in

branched versus straight channels as well (ratio close to 1). Similar trend was observed for the pure particle flow case for 100 nm particles (Fig. 9). When flowing along with the RBCs, a higher percentage of the 3  $\mu\text{m}$  particles get excluded in to the CFL based on size [86], compared to their 100 nm counterparts. At higher shear rates the RBCs tend to concentrate in the core region of flow while pushing out the 3  $\mu\text{m}$  particles of comparable size to the near wall CFL. This size based exclusion effect marginates more 3  $\mu\text{m}$  particles and brings more of the anti-ICAM-1 coated particles in contact with the ICAM-1 coated PDMS surface and produce almost two times higher binding density because of flow disturbances or alteration at the bifurcation [94-95].

100 nm particles show lower binding density compared to the 3  $\mu\text{m}$  particles at the 100  $\text{s}^{-1}$  shear rate with RBCs (Fig. 10). As explained before, size exclusion factor and increased collision to RBCs allows higher percentage of 3  $\mu\text{m}$  particles to come in contact with the wall surface and produce enhanced binding. Only a small percentage of 100 nm particles marginates to the near wall region while most of them still tend to flow along with RBCs in the core region because of their smaller size or they flow within the CFL as explained before. With an increase in shear rate less number of 100 nm particles comes in contact with the wall surface and there is less probability for binding. These factors lead to decrease in particle binding density for 100 nm particles compared to 3  $\mu\text{m}$  particles at higher shear rates when flowing with RBCs. The RBC 40% case produce higher binding density for 100 nm particles at low shear rates while the bigger 3  $\mu\text{m}$  particles shows better binding density at higher shear rate.

## Chapter: 4 Conclusions

The binding density of anti-ICAM-1 coated particles of 100 nm and 3  $\mu\text{m}$  size on ICAM-1 modified PDMS microfluidic devices is characterized in this work. The study employs various factors that influence particle distribution and binding such as RBCs, particle size, vessel geometry and shear rates.

RBCs play a major role in binding and distribution pattern of both 100 nm and 3  $\mu\text{m}$  particles. Based on the test results, it is found that RBCs enhance particle binding. 100 nm particles showed  $\sim 10$  fold increase in binding at low shear rates when compared to the pure particle case. Similarly, 3  $\mu\text{m}$  particles showed  $\sim 200$  fold increase in binding at high shear rates compared to the pure particle flow case. With variation in flow shear rate the CFL thickness changes. This is induced by margination of particles to the near wall CFL, which is influenced by shear rate. Axial-migration/tumbling motion of RBCs excludes particles to the CFL, leading to a non-uniform particle distribution. Based on the size exclusion factor, higher percentage of 3  $\mu\text{m}$  particles marginates towards the CFL compared to the 100 nm particles. Once in the CFL, RBC mediated collision of 3  $\mu\text{m}$  particles to the wall surface also enhances the binding probability. Because of their smaller size, the effect of size exclusion factor is low on 100 nm particles.

The 100 nm particles exhibit higher binding density compared to 3  $\mu\text{m}$  particles at all shear rates for the pure particle case. The particle binding density decreases with an increase in shear rate. Based on the particle size the force acting on them varies with shear rate. The smaller 100 nm particles have much lower drag force acting on them compared to the 3  $\mu\text{m}$  particles and therefore better probability for the ICAM-1 based

ligand-receptor binding to occur. Also the smaller 100 nm particles exhibit better diffusion to the wall region compared to the 3  $\mu\text{m}$  particles.

In terms of vessel geometry, 100 nm particles show slight increase in binding density at the branch channels compared to the straight channels for both pure particle and RBC 40% case. Similar pattern is shown by 3  $\mu\text{m}$  particles for the pure particle case. For the RBC 40% case the 3  $\mu\text{m}$  particle exhibit higher binding density at the branching section of the channel compared to the straight channels. This trend increases with shear rate and almost reaches 2 fold at 100  $\text{s}^{-1}$  shear rate.

These results help to determine the transport properties of drug carriers in the microvasculature. From this work we conclude that better drug delivery is attained in low shear rate sections of microvasculature by NP sized carriers. Whereas for achieving better drug delivery in microvasculature sections of high shear rate, microparticles of platelet size range would be a more suitable candidate. On choosing the right size range, better bioavailability and enhanced targeted binding of the drugs is achieved. This will provide higher efficacy and minimal drug dosage.

## Chapter: 5 Future Work

The current work is part of a big project to develop customized biomimetic microfluidic experimental platform that mimics specific microvasculature conditions based on disease state and physiological spot of origin. The project is to be taken to the next level by engineering the microfluidic channels to mimic vascular morphology by coating them with endothelial cells. The endothelial cell layer is to mimic disease condition by introducing required cytokines. This allows the expression of the corresponding disease specific biomolecules. A more physiologically relevant test condition can be set up for studying nano/micro drug carrier distribution and binding.

The testing platform can be extended for studying particle drug delivery in organs like lungs where the microvasculature is under periodic deformation during the breathing process. Periodically stretching microfluidic platforms will help in studying if the strain caused by the stretching effect has any role to play in particle drug distribution. The introduction of pulsatile flow, blood flow pattern observed *in vivo* is also to be considered. Thereby the current microfluidic device can be engineered into a universal platform for examining nano/micro drug particle delivery in physiologically relevant conditions.

## References

1. Manz, A., et al., *Planar chips technology for miniaturization and integration of separation techniques into monitoring systems: Capillary electrophoresis on a chip*. Journal of Chromatography A, 1992. **593**(1–2): p. 253-258.
2. Ng, J.M.K., et al., *Components for integrated poly(dimethylsiloxane) microfluidic systems*. ELECTROPHORESIS, 2002. **23**(20): p. 3461-3473.
3. Whitesides, G.M. and A.D. Stroock, *Flexible Methods for Microfluidics*. Physics Today, 2001. **54**(6): p. 42-48.
4. McDonald, J.C., et al., *Fabrication of microfluidic systems in poly(dimethylsiloxane)*. ELECTROPHORESIS, 2000. **21**(1): p. 27-40.
5. Hansen, C.L., et al., *A robust and scalable microfluidic metering method that allows protein crystal growth by free interface diffusion*. Proceedings of the National Academy of Sciences, 2002. **99**(26): p. 16531-16536.
6. Zheng, B., et al., *A Droplet-Based, Composite PDMS/Glass Capillary Microfluidic System for Evaluating Protein Crystallization Conditions by Microbatch and Vapor-Diffusion Methods with On-Chip X-Ray Diffraction*. Angewandte Chemie International Edition, 2004. **43**(19): p. 2508-2511.
7. Dittrich, P.S. and A. Manz, *Lab-on-a-chip: microfluidics in drug discovery*. Nat Rev Drug Discov, 2006. **5**(3): p. 210-218.
8. Pihl, J., M. Karlsson, and D.T. Chiu, *Microfluidic technologies in drug discovery*. Drug Discovery Today, 2005. **10**(20): p. 1377-1383.
9. Ramsey, R.S. and J.M. Ramsey, *Generating Electrospray from Microchip Devices Using Electroosmotic Pumping*. Analytical Chemistry, 1997. **69**(6): p. 1174-1178.
10. Sia, S.K. and G.M. Whitesides, *Microfluidic devices fabricated in Poly(dimethylsiloxane) for biological studies*. ELECTROPHORESIS, 2003. **24**(21): p. 3563-3576.
11. Werdich, A.A., et al., *A microfluidic device to confine a single cardiac myocyte in a sub-nanoliter volume on planar microelectrodes for extracellular potential recordings*. Lab on a Chip, 2004. **4**(4): p. 357-362.
12. Wheeler, A.R., et al., *Microfluidic Device for Single-Cell Analysis*. Analytical Chemistry, 2003. **75**(14): p. 3581-3586.
13. Dittrich, P.S. and A. Manz, *Single-molecule fluorescence detection in microfluidic channels—the Holy Grail in  $\mu$ TAS?* Analytical and Bioanalytical Chemistry, 2005. **382**(8): p. 1771-1782.
14. Stavis, S.M., et al., *Single molecule studies of quantum dot conjugates in a submicrometer fluidic channel*. Lab on a Chip, 2005. **5**(3): p. 337-343.
15. Gañán-Calvo, A.M. and J.M. Gordillo, *Perfectly Monodisperse Microbubbling by Capillary Flow Focusing*. Physical Review Letters, 2001. **87**(27): p. 274501.
16. Garstecki, P., et al., *Formation of monodisperse bubbles in a microfluidic flow-focusing device*. Applied Physics Letters, 2004. **85**(13): p. 2649-2651.
17. Thorsen, T., et al., *Dynamic Pattern Formation in a Vesicle-Generating Microfluidic Device*. Physical Review Letters, 2001. **86**(18): p. 4163-4166.
18. Link, D.R., et al., *Geometrically Mediated Breakup of Drops in Microfluidic Devices*. Physical Review Letters, 2004. **92**(5): p. 054503.

19. Xu, S., et al., *Generation of Monodisperse Particles by Using Microfluidics: Control over Size, Shape, and Composition*. Angewandte Chemie International Edition, 2005. **44**(5): p. 724-728.
20. Polla, D.L., et al. *MEMS-based diagnostic microsystems*. in *Microtechnologies in Medicine and Biology, 1st Annual International, Conference On*. 2000. 2000.
21. Holmes, D. and S. Gawad, *The Application of Microfluidics in Biology*. 2008. p. 55-80.
22. Wu, H.-W., C.-C. Lin, and G.-B. Lee, *Stem cells in microfluidics*. Biomicrofluidics, 2011. **5**(1): p. 013401.
23. Molloy, J.E. and M.J. Padgett, *Lights, action: Optical tweezers*. Contemporary Physics, 2002. **43**(4): p. 241-258.
24. Chris K. Fuller , J.H., Harold Ackler , Peter Krulevitch , Adam Eldredge , Frederick Becker , Jun Yang , Peter Gascoyne, *Microfabricated multi-frequency particle impedance characterization system*. Micro TAS 2000, 2000.
25. Holmes, D., H. Morgan, and N.G. Green, *High throughput particle analysis: Combining dielectrophoretic particle focussing with confocal optical detection*. Biosensors and Bioelectronics, 2006. **21**(8): p. 1621-1630.
26. Jonathan Leach, G.S., Pamela Jordan, Johannes Courtial, Miles Padgett, Jon Cooper, and Zsolt Laczik, *3D manipulation of particles into crystal structures using holographic optical tweezers*. Opt. Express 2004. **12**: p. 220-226.
27. Ceriotti, L., N.F. de Rooij, and E. Verpoorte, *An Integrated Fritless Column for On-Chip Capillary Electrochromatography with Conventional Stationary Phases*. Analytical Chemistry, 2002. **74**(3): p. 639-647.
28. Ros, A., et al., *Protein purification by Off-Gel electrophoresis*. PROTEOMICS, 2002. **2**(2): p. 151-156.
29. Macounová, K., et al., *Generation of Natural pH Gradients in Microfluidic Channels for Use in Isoelectric Focusing*. Analytical Chemistry, 2000. **72**(16): p. 3745-3751.
30. Sia, S.K., et al., *An Integrated Approach to a Portable and Low-Cost Immunoassay for Resource-Poor Settings*. Angewandte Chemie International Edition, 2004. **43**(4): p. 498-502.
31. Cesaro-Tadic, S., et al., *High-sensitivity miniaturized immunoassays for tumor necrosis factor [small alpha] using microfluidic systems*. Lab on a Chip, 2004. **4**(6): p. 563-569.
32. Cho, J.-H., et al., *Plastic ELISA-on-a-Chip Based on Sequential Cross-Flow Chromatography*. Analytical Chemistry, 2006. **78**(3): p. 793-800.
33. Liu, W.-T., et al., *Microfluidic device as a new platform for immunofluorescent detection of viruses*. Lab on a Chip, 2005. **5**(11): p. 1327-1330.
34. Psaltis, D., S.R. Quake, and C. Yang, *Developing optofluidic technology through the fusion of microfluidics and optics*. Nature, 2006. **442**(7101): p. 381-386.
35. Yager, P., et al., *Microfluidic diagnostic technologies for global public health*. Nature, 2006. **442**(7101): p. 412-418.
36. Copeland, R.A., D.L. Pompliano, and T.D. Meek, *Drug-target residence time and its implications for lead optimization*. Nat Rev Drug Discov, 2006. **5**(9): p. 730-739.
37. Langer, R., *Drug Delivery and Targeting*. Nature, 1998. **392**: p. 9-10.

38. Packhaeuser, C.B., et al., *In situ forming parenteral drug delivery systems: an overview*. European Journal of Pharmaceutics and Biopharmaceutics, 2004. **58**(2): p. 445-455.
39. Greg Light, S.S., Eun-Jung Park, Denise Drane, *Student understanding of "surface-area-to-volume ratio" and its relationship to property change in the nano-science engineering context*. 2010.
40. Suri, S., H. Fenniri, and B. Singh, *Nanotechnology-based drug delivery systems*. Journal of Occupational Medicine and Toxicology, 2007. **2**(1): p. 16.
41. Shah, S., et al., *Modeling Particle Shape-Dependent Dynamics in Nanomedicine*. Journal of Nanoscience and Nanotechnology, 2011. **11**(2): p. 919-928.
42. Haun, J.B. and D.A. Hammer, *Quantifying Nanoparticle Adhesion Mediated by Specific Molecular Interactions*. Langmuir, 2008. **24**(16): p. 8821-8832.
43. Kona, S., et al., *Biodegradable nanoparticles mimicking platelet binding as a targeted and controlled drug delivery system*. International Journal of Pharmaceutics, (0).
44. <http://www.thefreedictionary.com/microvasculature>.
45. Doshi, N., et al., *Flow and adhesion of drug carriers in blood vessels depend on their shape: A study using model synthetic microvascular networks*. Journal of Controlled Release, 2010. **146**(2): p. 196-200.
46. Fåhræus, R. and T. Lindqvist, *The Viscosity of the blood in narrow capillary tubes*. American Journal of Physiology -- Legacy Content, 1931. **96**(3): p. 562-568.
47. YANG, B.H., et al., *Migration of a sphere in tube flow*. Journal of Fluid Mechanics, 2005. **540**: p. 109-131.
48. Segré, G. and A. Silberberg, *Behaviour of macroscopic rigid spheres in Poiseuille flow Part 2. Experimental results and interpretation*. Journal of Fluid Mechanics, 1962. **14**(01): p. 136-157.
49. Harry L, G., *The microcirculatory society Eugene M. Landis award lecture: The microrheology of human blood*. Microvascular Research, 1986. **31**(2): p. 121-142.
50. Kim, S., et al., *The cell-free layer in microvascular blood flow*. Biorheology, 2009. **46**(3): p. 181-189.
51. McHedlishvili, G. and N. Maeda, *Blood Flow Structure Related to Red Cell Flow: Determinant of Blood Fluidity in Narrow Microvessels*. The Japanese Journal of Physiology, 2001. **51**(1): p. 19-30.
52. Pries, A.R., T.W. Secomb, and P. Gaehtgens, *Biophysical aspects of blood flow in the microvasculature*. Cardiovascular Research, 1996. **32**(4): p. 654-667.
53. William I, R., *Ratio of red cell velocities near the vessel wall to velocities at the vessel center in cerebral microcirculation, and an apparent effect of blood viscosity on this ratio*. Microvascular Research, 1972. **4**(1): p. 98-101.
54. Reinke, W., P. Johnson, and P. Gaehtgens, *Effect of shear rate variation on apparent viscosity of human blood in tubes of 29 to 94 microns diameter*. Circulation Research, 1986. **59**(2): p. 124-132.
55. Gaehtgens, P., H.J. Meiselman, and H. Wayland, *Velocity profiles of human blood at normal and reduced hematocrit in glass tubes up to 130  $\mu$  diameter*. Microvascular Research, 1970. **2**(1): p. 13-23.



56. Yasuhiko Sugii, S.N., Koji Okamoto, *In vivo PIV measurement of red blood cell velocity field in microvessels considering mesentery motion*. Physiological Measurement, 2002. **23**(2).
57. Nanne, E.E., C.P. Aucoin, and E.F. Leonard, *Shear Rate and Hematocrit Effects on the Apparent Diffusivity of Urea in Suspensions of Bovine Erythrocytes*. ASAIO Journal, 2010. **56**(3): p. 151-156 10.1097/MAT.0b013e3181d4ed0f.
58. Aarts, P., R. Heethaar, and J. Sixma, *Red blood cell deformability influences platelets--vessel wall interaction in flowing blood*. Blood, 1984. **64**(6): p. 1228-1233.
59. Goldsmith, H.L. and S.G. Mason, *Particle motions in sheared suspensions XIII. The spin and rotation of disks*. Journal of Fluid Mechanics, 1962. **12**(01): p. 88-96.
60. Mayrovitz, H.N., R.F. Tuma, and M.P. Wiedeman, *Relationship between microvascular blood velocity and pressure distribution*. American Journal of Physiology - Heart and Circulatory Physiology, 1977. **232**(4): p. H400-H405.
61. Gimbrone, M.A., T. Nagel, and J.N. Topper, *Biomechanical activation: an emerging paradigm in endothelial adhesion biology*. The Journal of Clinical Investigation, 1997. **99**(8): p. 1809-1813.
62. Zhai, Y., et al., *LIGHT, a novel ligand for lymphotoxin beta receptor and TR2/HVEM induces apoptosis and suppresses in vivo tumor formation via gene transfer*. The Journal of Clinical Investigation, 1998. **102**(6): p. 1142-1151.
63. Min, J.-K., et al., *TNF-Related Activation-Induced Cytokine Enhances Leukocyte Adhesiveness: Induction of ICAM-1 and VCAM-1 via TNF Receptor-Associated Factor and Protein Kinase C-Dependent NF- $\kappa$ B Activation in Endothelial Cells*. The Journal of Immunology, 2005. **175**(1): p. 531-540.
64. Kanwar, J.R., et al., *Requirements for ICAM-1 immunogene therapy of lymphoma*. Cancer Gene Ther, 2003. **10**(6): p. 468-476.
65. Hiroaki Tanaka, M.Y., Takeshi Sunami, Masaichi Ohira, K. Hirakawa-Y.S. Chung, *Lipid-mediated gene transfection of intercellular adhesion molecule-1 suppresses the peritoneal metastasis of gastric carcinoma*. International Jpournal of Molecular Medicine, 2002. **10**(5).
66. McDonald, J.C. and G.M. Whitesides, *Poly(dimethylsiloxane) as a Material for Fabricating Microfluidic Devices*. Accounts of Chemical Research, 2002. **35**(7): p. 491-499.
67. Koval, M., et al., *Size of IgG-Opsonized Particles Determines Macrophage Response during Internalization*. Experimental Cell Research, 1998. **242**(1): p. 265-273.
68. Andres J. Calderon, V.M., Silvia Muro, David M. Eckmann, *Flow dynamics, binding and detachment of spherical carriers targeted to ICAM-1 on endothelial cells*. Biorheology, 2009. **46**: p. 323-341.
69. Elisabetta Canetta, A.D., Anne Leyrat, Claude Verdier, *Measuring cell viscoelastic properties using a force-spectrometer: Influence of protein-cytoplasm interactions*. Biorheology, 2005. **42**(5/2005): p. 321-333.
70. Decuzzi, P. and M. Ferrari, *The adhesive strength of non-spherical particles mediated by specific interactions*. Biomaterials, 2006. **27**(30): p. 5307-14.

71. Ganong, W.F., *Review of Medical Physiology*. 21st ed. 2003, New York: Lange Medical Books/McGraw-Hill Medical Publishing Division.
72. G Keren, J.S., R Megidish, B Levitt, *Pulmonary venous flow pattern--its relationship to cardiac dynamics. A pulsed Doppler echocardiographic study*. *Circulation*, 1985. **71**: p. 1105-1112.
73. Lipowsky, H., S. Kovalcheck, and B. Zweifach, *The distribution of blood rheological parameters in the microvasculature of cat mesentery*. *Circulation Research*, 1978. **43**(5): p. 738-749.
74. Milnor WR. Hemodynamics. Williams and Wilkins, B., USA. , 1982; 53 pp.
75. Popel AS, J.P., *Microcirculation and hemorheology*. *Annual Review of Fluid Mechanics*, 2005. **37**: p. 43–69.
76. Ho Seong Ji, J.Y.L.a.S.J.L., *In-vitro study on the hemorheological characteristics of chicken blood in microcirculation*. *Rheology Journal*, 2007. **19**: p. 89-95.
77. Goldsmith HL, M.S., *The microrheology of dispersions*. In *Rheology, Theory, and Applications*. FR Eirich, Ed. Academic Press, New York, 1967. **4**: p. 85-250.
78. Ham, A.S.W., et al., *Microparticle adhesive dynamics and rolling mediated by selectin-specific antibodies under flow*. *Biotechnology and Bioengineering*, 2007. **96**(3): p. 596-607.
79. Kameneva, M.V., *Blood soluble drag-reducing polymers prevent lethality from hemorrhagic shock in acute animal experiments*. *Biorheology*, 2004. **41**: p. 53-64.
80. Kim, S., et al., *Temporal and spatial variations of cell-free layer width in arterioles*. *American Journal of Physiology - Heart and Circulatory Physiology*, 2007. **293**(3): p. H1526-H1535.
81. Blasberg P, W.L.J., Schmid-Schonbein H, *Microrheology of thrombocyte deposition. Effect of stimulation, flow direction and red cells*. In *Fluid dynamics as a localizing factor for atherosclerosis Schettler G, Nerem RM, Schmid-Schonbein M, Morl H, Diehm C, eds*. Berlin: Springer-Verlag, 1983: p. 103-114.
82. Weiss HJ, T.V., Baumgartner HR, *Role of shear rate and platelets in promoting fibrin formation on rabbit subendothelium. Studies utilizing patients with quantitative and qualitative platelet defects*. *J Clin Invest.*, 1986. **78**(4): p. 1072–82.
83. Aarts, P., et al., *Blood platelets are concentrated near the wall and red blood cells, in the center in flowing blood*. *Arteriosclerosis, Thrombosis, and Vascular Biology*, 1988. **8**(6): p. 819-824.
84. Gerard B. Nash, T.W., Colin Thornton, Mostafa Barigou, *Red cell aggregation as a factor influencing margination and adhesion of leukocytes and platelets* *Clinical Hemorheology and Microcirculation* 2008. **39**(1-4): p. 303-310.
85. Gentile, F., et al., *The margination propensity of spherical particles for vascular targeting in the microcirculation*. *Journal of Nanobiotechnology*, 2008. **6**(1): p. 9.
86. Charoenphol, P., R.B. Huang, and O. Eniola-Adefeso, *Potential role of size and hemodynamics in the efficacy of vascular-targeted spherical drug carriers*. *Biomaterials*, 2010. **31**(6): p. 1392-1402.
87. Melder, R.J., et al., *Selectin- and integrin-mediated T-lymphocyte rolling and arrest on TNF-alpha-activated endothelium: augmentation by erythrocytes*. *Biophysical Journal*, 1995. **69**(5): p. 2131-2138.

88. Eckstein, E.C., A.W. Tilles, and F.J. Millero Iii, *Conditions for the occurrence of large near-wall excesses of small particles during blood flow*. *Microvascular Research*, 1988. **36**(1): p. 31-39.
89. Sharan, M. and A.S. Popel, *A two-phase model for flow of blood in narrow tubes with increased effective viscosity near the wall*. *Biorheology*, 2001. **38**(5): p. 415-428.
90. Turitto, V., A. Benis, and E. Leonard, *Platelet Diffusion in Flowing Blood*. *Industrial & Engineering Chemistry Fundamentals*, 1972. **11**(2): p. 216-223.
91. P Decuzzi, F.G., A Granaldi, A Curcio, F Causa, *Flow chamber analysis of size effects in the adhesion of spherical particles*. *International Journal of Nanomedicine*, 2007. **2**(4): p. 689 - 696.
92. V R Shinde Patil, C.J.C., Y H Yun, S M Slack, and D J Goetz, *Particle diameter influences adhesion under flow*. *Biophys Journal*, 2001. **80**(4): p. 1733-1743.
93. Goldman, A.J., R.G. Cox, and H. Brenner, *Slow viscous motion of a sphere parallel to a plane wall—II Couette flow*. *Chemical Engineering Science*, 1967. **22**(4): p. 653-660.
94. Zhang Z, K.C., Donohue JF, Kim CS, *Comparison of micro- and nano-size particle depositions in a human upper airway model*. *J Aerosol Sci*, 2005. **36**: p. 211-233.
95. Prabhakarandian, B., et al., *Bifurcations: Focal Points of Particle Adhesion in Microvascular Networks*. *Microcirculation*, 2011. **18**(5): p. 380-389.

## VITA

Antony Thomas was born in Kerala, India. He completed his high school from Girideepam Central School, Kerala and entered Sathyabama University, Chennai for doing his Undergraduate studies in August 2004. He received his Bachelor of Technology degree in Biomedical Engineering in May 2008. After working for about an year, he entered the University of Texas at Arlington to do his Masters in Bioengineering in August 2009. During August 2010, he transferred to Lehigh University, PA and continued his Graduate studies in the Bioengineering Program. In May 2012 he will be awarded a Master of Science degree in Bioengineering form Lehigh University, Bethlehem, PA on completion of the requirements.

Permanent address: 411 E Morton St

Bethlehem, PA 18015

Email: ant210@lehigh.edu